DESIGN OF AN IN VIVO ROBOTIC PLASMA MEDICINE DEVICE

A Thesis

by

BROOKS NOLAN MCKINNEY

Submitted to the Office of Graduate and Professional Studies of
Texas A&M University
in partial fulfillment of the requirements for the degree of

MASTER OF SCIENCE

Chair of Committee,	Dr. Seok Chang Ryu
Committee Members,	Dr. David Staack
	Dr. Michael Moreno
Head of Department,	Dr. Andreas A. Polycarpou

August 2019

Major Subject: Mechanical Engineering

ABSTRACT

This research explored the design and feasibility of a robotic plasma medicine device intended for cancer treatment inside of the human body, potentially enabling the delivery of cold atmospheric plasma in a safe, controllable, and minimally invasive manner. A dielectric barrier discharge (DBD) plasma jet was generated using a device consisting of two ring electrodes, a borosilicate glass tube, epoxy insulation, and a grounded outer shield. For the feasibility study, three different plasma jet devices with insulation thicknesses of 3.5 mm, 4.5 mm. and 5.5 mm, corresponding to outer device diameters of 16 mm, 18 mm, and 20 mm were manufactured and investigated. The electrical and thermal safety of devices was evaluated under high voltage operating conditions following a standardized Test to Breakdown, Step-by-Step method and measuring the device outer surface temperature using a fiber Bragg grating (FBG) optical sensor. Breakdown voltage increased with insulation thickness, and all devices tested failed above 11 kV. The rate of device temperature increase decreased with an increase in insulation thickness. However, the tested devices would only be safe to generate plasma in vivo for approximately a minute or less, depending on insulation thickness and voltage. Consistent manufacturing, along with eliminating any air voids in insulation is critical to device safety. A full-scale, functional robotic plasma jet device (3.5 mm insulation thickness, 16 mm outer diameter) with a robotic interface compatible with the current dA Vinci robotic surgical system was also designed and manufactured. It was demonstrated that a plasma plume is capable of being successfully delivered through a dynamically moving, steerable distal tip that is operated by a robotic system.

ACKNOWLEDGMENTS

I would like to thank my advisor, Dr. Ryu for his guidance, support, and feedback throughout my graduate research as well as for the opportunity to work on this project. Special thank you to Dr. Staack, Matthew Burnette, and Chris Campbell from the Plasma Engineering and Diagnostics Laboratory for helping with the experimental setup design, electrical diagnostics using the oscilloscope, 3D printing parts for the plasma device and robotic system, and providing feedback. Thank you to Rohith Karthikeyan, Taimoor Khan, Shivanand Pattanshetti, Harsha Mohan, and Will McKinney for assisting with device testing. I would like to express my appreciation to Dr. Moreno for his review and feedback. In addition, I would also like to thank my parents for their continuous support throughout my graduate studies.

CONTRIBUTORS AND FUNDING SOURCES

Contributors

This work was supported by a thesis committee consisting of Dr. Ryu and Dr. Staack of the Department of Mechanical Engineering and Dr. Moreno of the Department of Biomedical Engineering. All work conducted for the thesis was completed by the student independently.

Funding Sources

Graduate study was not supported by any funding sources.

TABLE OF CONTENTS

Page

LIST OF FIGURES

FIGURE Page

LIST OF TABLES

TABLE Page

1. INTRODUCTION

1.1 Cancer Overview

1.1.1 Cancer

Cancer is a collection of related diseases in which some of the body's cells proliferate uncontrollably [8]. Cancerous tumors are malignant, which means they can invade surrounding tissues or travel to distant locations in the human body far from where they originate. Normal cells undergo a programmed cell death process known as apoptosis to discard of unneeded cells that are damaged or old. On the contrary, cancer cells are able to ignore these apoptosis signals, leading to abnormal cell division without regulation and dispersion into nearby tissues [8]. More than 100 types of cancers exist, along with various treatment options.

Cancer is the second leading cause of death worldwide, accounting for an estimated 18.1 million new cases and 9.6 million deaths in 2018 [9]. The most commonly diagnosed cancers are lung, breast, colorectum, prostate, stomach, and liver. The highest number of mortalities and respective survival rates are from cancers of lung (18.6%), colorectum (64.5%), stomach (31.0%), liver (17.7%), breast (89.6%), esophagus (19.2%), pancreas (8.5%), and prostate (98.2%) [10].

1.1.2 Conventional Methods in Cancer Therapy and Limitations

Three general cancer treatment options, currently available, include surgery, radiation therapy, and systemic therapy. Each treatment method has advantages and disadvantages. Surgery often entails using microsurgical techniques such as lasers and laparoscopy to remove cancerous tumors that are still localized. Although one of the safest routes for cancer treatment, surgery can damage surrounding normal tissues to reach a tumor, affect patient quality of life with removal of an organ, or leave cancer cells behind inside the body [11, 12]. Radiation therapy directs a highly localized beam of high-energy waves at the targeted tumor in attempt to kill a large portion of cancer cells and shrink tumors [12]. Several disadvantages of radiation therapy include damage to surrounding tissues or organs depending on proximity to the tumor, inability to kill all cancer cells in larger

tumors, ineffectiveness in regions that lack good oxygen supply, and fatigue side effects [11]. Systemic therapy, such as chemotherapy, utilizes medications that are generally administered through a vein, by mouth, or into a muscle to kill rapidly growing and dividing cancer cells. These drugs travel throughout the entire body and attack widespread cancers [12]. However, systemic therapy eradicates cancer cells in a relatively uneven manner and also destroys healthy cells, causing toxic side effects. Side effects include hair loss, nausea, fatigue, and destruction of the immune system [12]. Another common issue of chemotherapy and radiation is that sometimes, they must be delivered frequently, for an extended period of time. These conventional treatment methods are often used in combination with each other to increase effectiveness. They can be expensive, accompanied by serious side effects, induce damage to nearby healthy tissues, and reach a saturation level of their efficacy. Furthermore, cancer cells can develop a resistance to treatments over time, becoming unbeneficial to the patient [13]. Each cancer type is unique in which it presents its own set of treatment challenges and requires a specific treatment regimen that depends on various factors including the patient, tumor location, accessibility, size, and stage of cancer. Therefore, alternative treatments are needed in the quest to cure cancer more effectively.

1.2 Cold Atmospheric Plasma

1.2.1 Background and Applications

Plasma represents the fourth state of matter [14]. This highest energy state of matter is an ionized gas composed of free moving electrically charged particles in the form of electrons and ions, as well as neutral molecules. Plasma is highly electrically conductive, and electric and magnetic fields influence the behavior of the matter. Plasma can be classified into two different regimes according to the relative temperatures of the electrons, ions, and neutrals: 1. Thermal or hot and 2. Non-thermal or cold. Thermal plasmas are in thermal equilibrium in which electrons and heavy species are at the same temperature, while in non-thermal plasma (NTP), hot electrons and cold neutral gas ions coexist in a non-equilibrium plasma state [15].

NTP is a collection of reactive constituents including charged species, excited neutral species,

visible, ultraviolet, and infrared radiation, and other electromagnetic fields, as shown in Figure 1.1 [16]. Cold atmospheric plasma (CAP), also known as low temperature plasma (LTP), is operated at atmospheric pressure, and the gas remains close to room temperature. These attractive features make NTP sources suitable for many microfabrication industrial applications such as material processing, surface modification and etching, and chemical vapor deposition [13, 17]. CAPs can also be safely applied to heat-sensitive biological substrates such as living cells and tissues without causing thermal damage, attractive for therapeutic purposes in the field of plasma medicine.

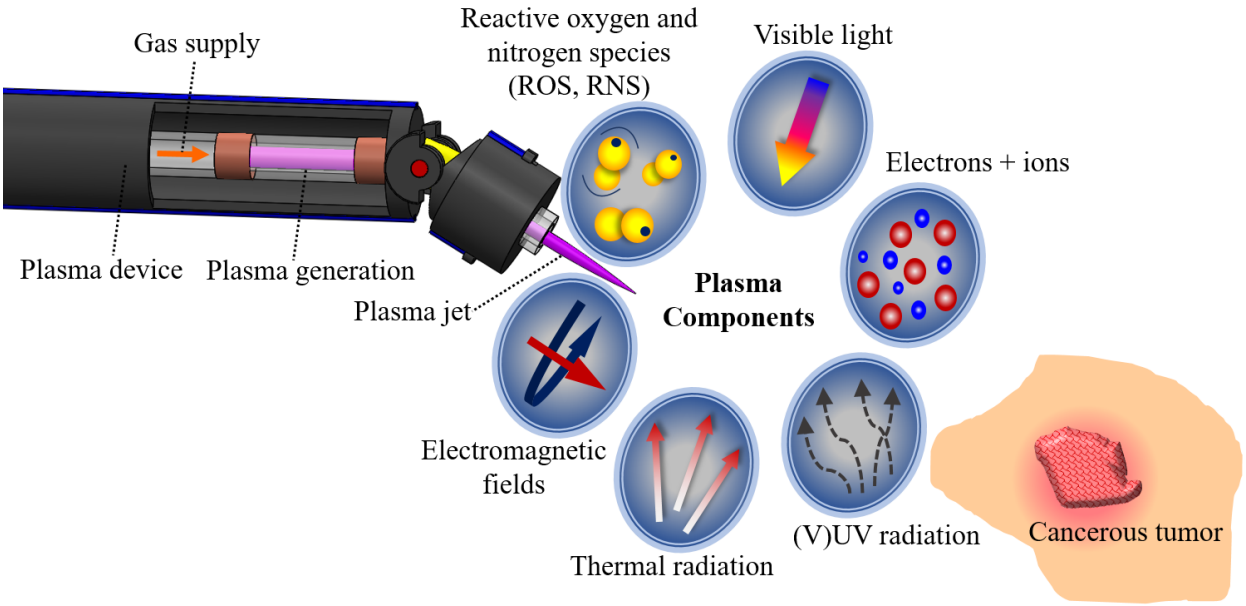

Figure 1.1: Cold atmospheric plasma jet containing a mixture of reactive components target a cancerous tumor.

Plasma medicine represents the scientific discipline associated with the direct application of CAP on or inside the human body for bio-medical applications [18]. Some major areas of this novel discipline include microbial decontamination and sterilization, dental care, wound healing and blood coagulation, treatment of skin diseases, and more recently cancer therapy [13].

1.2.2 Biological Effects and Mechanisms

According to concurring reports, three general biological effects of CAP have been identified that are relevant for medical purposes: (1) inactivation of a wide variety of microorganisms, including multiple drug resistant ones; (2) stimulation of cell proliferation as well as tissue regeneration, and (3) inactivation of mammalian cells, especially cancer cells, by induction of apoptosis [16, 18]. The specific biological effect, such as the difference between cell proliferation and inactivation, is dependent on the level of plasma treatment intensity or exposure time, in which apoptosis can be initialized by higher plasma treatment intensities [18]. Despite not being completely understood, two fundamental mechanisms behind these beneficial biological effects of CAP on living cells and tissues have emerged. Plasma biological responses are significantly triggered by plasma evoked alteration of the liquid environment of cells. Radicals and chemical products, specifically reactive oxygen and nitrogen species (ROS, RNS), that are produced in or transferred into liquid phases by plasma treatment play a dominating role [16, 18]. CAP has a synergistic effect on cells, creating pores and allowing better penetration of reactive species. The ROS cause oxidative stress and DNA damage to cells, leading to cancer cell apoptosis [19]. Other plasma components such as UV radiation and electric fields are believed to have more minor biological effects.

1.2.3 Anti-Cancer Effects and Limitations

The potential of LTP in terms of safety and effectiveness for cancer treatment has been recently explored. Studies have demonstrated that a CAP treatment can selectively kill cancer cells in vitro and also suppress cell growth, leading to tumor size reduction in vivo [13, 20]. CAP treatment has exhibited its significant anti-cancer effects on over 20 cancer types in vitro including brain, skin, breast, colorectal, lung, cervical, leukemia, hepatoma, and head and neck cancer [21]. The bulk of studies on CAP for cancer treatment have primarily focused on different cancer cell lines in vitro, skin diseases outside the body, and tumors in animal studies.

The merit of CAP is that a localized treatment can selectively eradicate various tumor cells without causing harm to surrounding, healthy tissue, when the proper dosage is applied [22, 4].

The plasma dose is a key factor on the effect on mammalian and cancer cells. The dose can be defined in terms of the duration of time over which the plasma is applied, and it is dependent on the plasma composition and purpose [1]. For lower plasma doses (low plasma intensity or short exposure time), observed effects included cell-surface detachment and inhibition of cell migration. However, the detached cells post plasma exposure remained alive, reattached to the surface again, and proliferated after a short incubation period. Higher plasma doses (higher plasma intensity or longer exposure time) caused either cell apoptosis, or at an additional exposure time, necrosis (accidental cell death) [13, 15]. Therefore, there is a dose-dependent effectiveness of plasma treatment that must be defined according to the desired outcome.

Despite the benefits of CAP for cancer treatment, limitations and issues still exist. The effectiveness of the treatment is largely dependent on being able to precisely control and deliver the appropriate plasma dose. The maximum penetration of plasma reactive species in tissues is only a few millimeters, potentially limiting the treatment depth for solid tumors inside the body [20, 23]. Atmospheric pressure plasma, in the conventional form, is not practical for inside the body use in clinical applications due to high voltage components, gas delivery, and size and rigidity of most plasma systems [4, 24]. The composition, relationship, and quantity of plasma components may vary significantly based on the plasma source configuration, working gas, and experimental setup, making it difficult to have a specific set of quantified parameters that would work universally for all plasma devices [16]. Therefore, operating parameters and appropriate plasma dosage must be well defined according to the specific plasma device and the targeted type of cancer.

1.2.4 Plasma Devices

LTP devices can generally be classified into three main categories: direct, indirect, and hybrid plasma sources. A number of plasma device parameters including the applied electrical inputs, plasma power, working gas mixture, geometry, and electrode configuration can be altered according to the desired application. Each plasma method has advantages and disadvantages depending on the application.

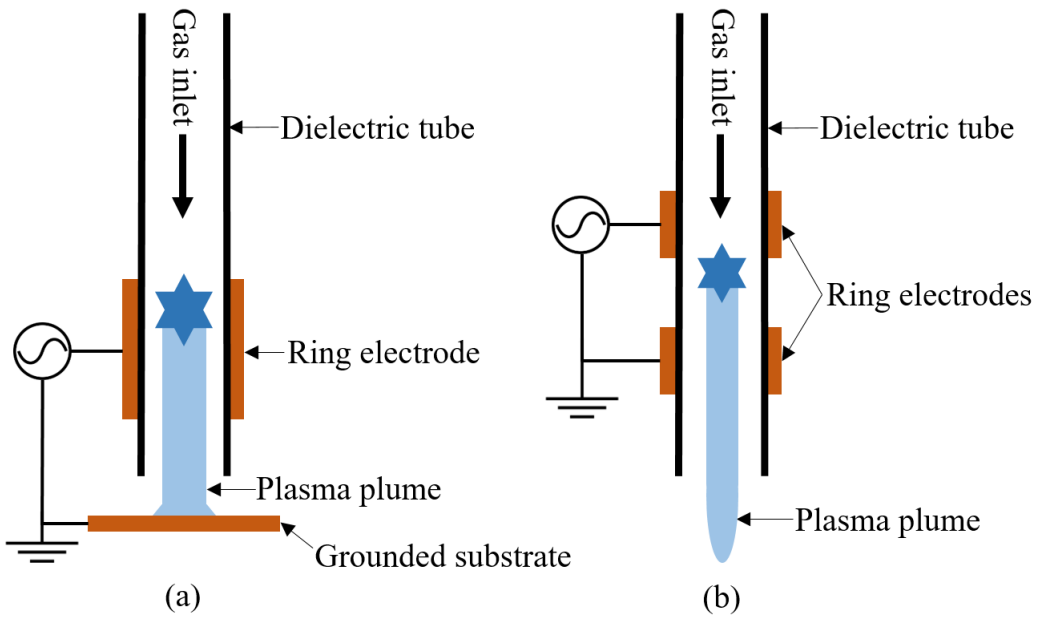

Figure 1.2: Schematics of LTP sources: (a) Direct plasma source with floating-electrode, (b) Indirect plasma source with 2 ring electrodes.

A direct plasma source, such as a floating-electrode dielectric barrier discharge (DBD) jet, utilizes a single, isolated powered electrode, and the substrate itself acts as the second electrode (grounded or at floating potential) (Figure 1.2(a)). Due to plasma being generated directly to the substrate, both excited species and charged species (electrons and ions) can be delivered to the surface [25]. For medical treatment, the human body or tissue functions as the counter electrode. A portion of the current passes through the body's living tissue, and this small conduction current is usually limited in order to minimize the thermal effects and electrical stimulation of muscles [20]. With the human body serving as the ground, the distance between the plasma device and substrate can effect plasma generation and stability, especially at farther distances. Thus, a fixed device-tissue distance is necessary for stable operation. Any variations in the targeted substrate's conductibility may also influence plasma ignition [18]. A direct plasma DBD has the ability to cover and treat large areas in comparison to an indirect plasma jet, which is more suitable for targeted, spot-like treatments [18].

An indirect method, also known as afterglow plasma, has a main discharge region in which

plasma generation is confined between two electrodes (high voltage electrode and grounded electrode), and the plasma plume is carried downstream or outside the device by gas flow (Figure 1.2(b)). Charged species typically flow to the second electrode instead of the substrate surface, resulting in fewer plasma species near the substrate compared to direct plasma [25]. However, due to the distance between electrodes being fixed for an indirect plasma device, plasma generation and stability is generally less effected by device position in relation to the substrate and any variations of surrounding environmental air conditions [18].

Hybrid plasma sources combine the generation technique of direct plasma with an afterglow plasma source, thus creating a current-free condition in the substrate or tissue. This configuration typically employs a grounded wire mesh electrode that has a smaller electrical resistance than that of the skin, ideally allowing all of the current to flow through the wire mesh [1, 20].

Existing plasma devices used in research and clinical applications were reviewed. Morfill et al. developed a large area scalable plasma dispenser designed for hand disinfection [2]. The 'HandPlaSter' prototype is shown in Figure 1.3(a). The design uses a hybrid, sandwich electrode configuration composed of a dielectric Teflon plate sandwiched between a HV copper electrode and a grounded mesh electrode. While generating plasma in the gaps between the wires of the mesh electrode, the device operates safety, with low power consumption and little increase in temperature.

Experimental studies by Kustov and associates have demonstrated the ability to remotely generate a cold atmospheric pressure plasma jet (APPJ) at the downstream end of a long, flexible plastic tube using a thin floating metal wire installed inside the tube for microbial decontamination (Figure 1.3(b)) [3, 4]. Although this setup allows for safe touch and easy manipulation without risk of electric shock, there are several limitations to consider for in vivo use. Plasma generation, gas discharge, and plume length can be influenced by conductive objects in contact with the tube wall and proximity of the substrate near the tube exit, which could also effect the stability of the plume and the ability to accurately control dosage, key aspects of selective cancer treatment (McKinney, Feasibility Study of In Vivo Robotic Plasma Medicine Devices, International Symposium

on Medical Robotics) © 2019 IEEE.

Cold atmospheric pressure plasma generation in long, flexible biopsy channels for inner-tube decontamination and medical applications using a direct plasma, DBD in a bifilar helix electrode configuration was reported by Polak and Winter [26]. The plasma device consist of an inner tube and an outer tube concentrically aligned as well an equidistant twisted powered and grounded electrode arrangement around the inner tube. Although capable of igniting a homogeneous discharge inside a 2 mm inner diameter (ID) tube, 5 m in length, and demonstrating microbicidal efficacy, erosion of the polytetrafluoroethylene (PTFE) tube material was observed. To elude erosion of this thermolabile tube, indirect plasmas or plasma bullets were suggested for possible consideration.

A popular commercially available plasma device that is CE-certified as a class IIa medical device is the kINPen MED (neoplas tools GmbH, Greifswald, Germany). The kINPen MED is an argon-driven cold atmospheric plasma jet device for the treatment of chronic wounds and pathogen-based skin diseases. This hand-held unit consist of a central rod electrode, a grounded ring electrode that is attached to a dielectric quartz capillary tube, and an outer metal housing as shown in Figure 1.3(c). The device has several innovative features including an integrated mass

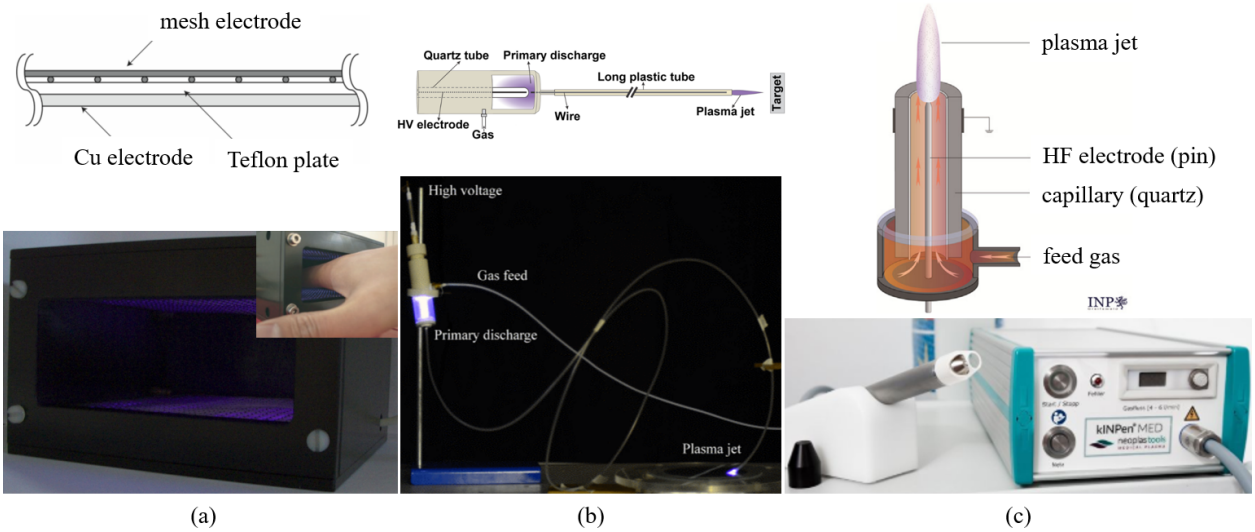

Figure 1.3: Existing plasma devices: (a) 'HandPlaSter' plasma dispenser prototype used for hand disinfection [1, 2], (b) Remote APPJ through long flexible tube [3, 4], (c) kINPen MED device (neoplas tools GmbH, Greifswald, Germany) [5, 6] (Reprinted from [6]).

flow controller, a gas curtain for control of ambient conditions and to prevent formation of flash-overs to the grounded electrode, and a sterilized distant piece or exchangeable spacer to maintain a safe working distance and patient hygiene [27, 28]. During treatment, the device is positioned perpendicular to the wound and moved across the affected region at a moderate consistent speed of 5 mm/s. The effective plasma treatment area of the kINPen MED covers about 1 cm^2 [6]. The plasma treatment intensity is controlled via the treatment time. Recommended physical properties and parameters including feed gas, flow rate, frequency, power, and working distance for the kINPen MED are defined in [27, 28]. These specified working parameters are necessary for clinical use. Several more prototypes based on the kINPen technology have emerged including a flexible plasma device for endoscopic, antibacterial applications and a hand-held dental instrument manageable to reach intricate anatomic regions [18].

There are several limitations of existing devices for plasma application inside the human body. Current devices, primarily designed for use outside the body, require manual control by hand and do not have a steerable tip. A controllable device capable of precisely delivering a plasma dose to a targeted tumor is essential to selectively treat cancer and a variety of tumor sizes inside the body.

1.3 High Voltage and Insulation

Since plasma devices use high voltage components (a power electrode), it is essential to be aware of electrical insulation and potential issues. There are numerous factors to examine when considering high voltage insulation methods. The main goal of high voltage design for plasma sources is to produce reliable breakdown where it is wanted and to prevent breakdown where it is undesired [29]. In this case, breakdown is desired inside the dielectric tube to generate and deliver plasma. On the other hand, breakdown is unwanted anywhere surrounding the electrodes, dielectric tube, and device exterior.

Unwanted discharges in high voltage systems can cause catastrophic failures. If an insulator contains any voids, the bulk of an insulator can fail for two main reasons. First, the reduced relative permittivity (dielectric constant) in the void increases the field inside the void. Second, the void is likely to contain a gas with a much lower dielectric strength than the primary insulator [29]. At an

electric field of about 3 kV/mm, air can begin to breakdown, becoming partially conductive [29]. Any air gaps, pockets, or bubbles surrounding high voltage components can promote localized partial discharges and lead to insulation degradation and breakdown [30].

Several insulating strategies can be implemented to increase the breakdown voltage between electrodes. The gap between electrodes and surrounding volume must be completely filled with an insulation material of high dielectric strength, while ensuring no voids are present. A popular technique to eliminate bubbles is vacuum injection molding. An insulating material homogeneous in characteristics is also ideal to ensure that the dielectric constant is the same throughout the insulation and allows for a more constant electric field strength gradient [30].

The electrode itself in terms of geometry and cleanliness also plays a critical role in the overall breakdown voltage of the system. High voltage electrodes should be physically smooth (both microscopically and macroscopically), highly polished, and have gently curving features to minimize surface irregularities that could cause localized field enhancements on a microscopic level [29]. The surfaces of the electrode and insulator should also be clean in which any dirt, grease, or water can promote tracking.

This knowledge of high voltage and insulating issues can be applied to the design and manufacturing of in vivo plasma devices to help prevent unwanted breakdowns.

1.4 Objectives

In order to help mitigate potential issues including high voltage safety, device size invasiveness, plasma stability, and plasma dosage control, this paper proposes a design of an insulated, robotic plasma medicine device, intended for in body cancer treatment, potentially enabling the delivery of plasma in a safe, controllable, and minimally invasive manner. A schematic of the proposed device and robotic system is shown in Figure 1.4.

The device has several design features that are important to its functionality for in vivo cancer treatment. The device is designed to generate and deliver a stable plasma plume through a steerable distal tip that is operable by a robotic system. The steerable distal tip will help control tip orientation and treat various tumor sizes. A vision-based joint angle estimation system allows

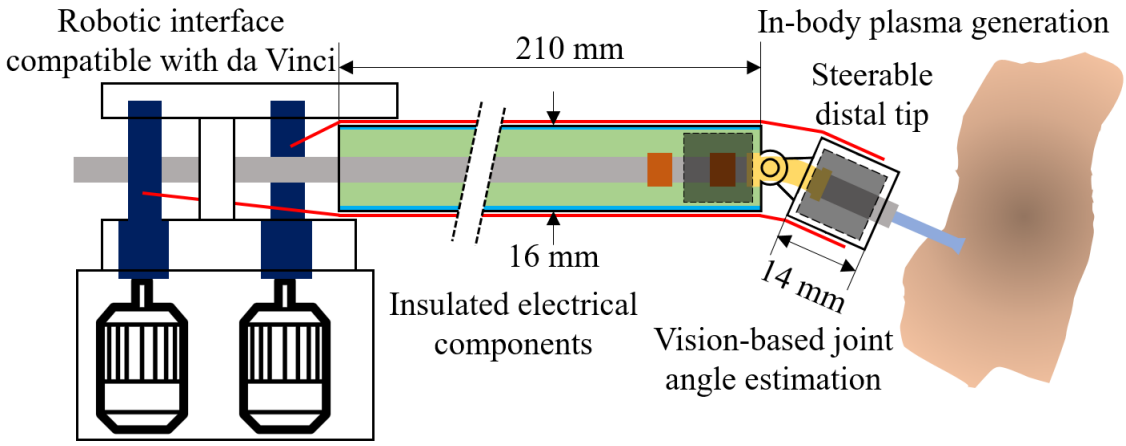

Figure 1.4: Schematic of insulated robotic plasma medicine device that is tendon actuated using servomotors along with key design features. Adapted from [7] © 2019 IEEE.

real-time tracking of tip position, angle, and angular velocity without being effected by any surrounding electromagnetic fields. The device allows for safe plasma generation inside the body with insulated electrical components. The robotic interface is compatible and controllable with an existing robotic surgical system, the da Vinci EndoWrist arm (Intuitive Surgical Inc., Sunnyvale, CA).

The intended application of the proposed device is to treat exposed cancers inside the body. In addition, this device could possibly be used in conjunction with surgical cancer treatments to help supplement its limitations and increase effectiveness. The surgical instruments could be treated by CAP during surgical operations to disinfect/decontaminate equipment, kill cancer cells, and prevent the spread of cancer elsewhere. Also, plasma treatment could applied around the edges of the tumor and after surgical procedures to kill any remaining microscopic disease.

The primary objective of this thesis was to design reliable and easily-controllable plasma devices that are tailored to different medical demands, specifically to treat many types of cancer. There are two main requirements for cold atmospheric plasma to be suitable for application directly onto or inside the human body. First, the plasma needs to operate stable, safe, and reproducible under open atmospheric conditions. Second, the plasma must be less than 40^{o}C at the tissue contact zone to prevent any thermal damage [18]. For cancer therapies, it is important to be able to pre-

cisely control both the dose of plasma being delivered to the targeted tumor and the treatment area in such a way to selectively destroy cancer cells while preserving normal, surrounding tissue. A robust design process is necessary in designing and testing plasma devices for in vivo applications to ensure safe, reproducible, and precise plasma delivery.

The following objectives were defined to justify this study:

1. Design a robotic plasma medicine device intended for safe, in-body cancer treatment
    (a) Define necessary design requirements, features, and components
    (b) Identify materials/dimensions and develop a manufacturing process
2. Investigate the safety of plasma devices during plasma generation using experimental testing
    (a) Insulation testing- determine the effect of insulation thickness and applied voltage on breakdown voltage and failure
    (b) Temperature testing- determine the effect of insulation thickness on the device temperature increase over time at an applied voltage
3. Demonstrate the feasibility of a functional robotic plasma medicine device
    (a) Design and build a functional prototype
    (b) Deliver a plasma plume through a moving distal tip
    (c) Evaluate feasibility of device according to satisfaction of design requirements

This thesis explored the feasibility of in vivo robotic plasma medicine devices in terms of design, manufacturing, safety, and functionality. The design process and experimental testing can provide a basis for practical guidelines to consider in development of LTP cancer treatment technology. The results can help define an operating voltage range and operating time limit for safe, in-body use by surgeons. With the proposed device and its steerable distal tip, the plasma plume and appropriate dose can be precisely controlled and delivered to treat normal sized tumors.

The rest of the paper is organized as follows. Section 2 presents the design and prototyping process, Section 3 evaluates the electrical and thermal insulation using experimental testing of several prototypes, followed by results and discussion in Section 4, and conclusions in Section 5.

2. DEVICE DESIGN AND PROTOTYPING

2.1 Plasma Device Design

2.1.1 Design Overview and Components

Prior to selecting an insulating method or material, preliminary testing of a device without insulation during plasma generation revealed two locations most susceptible to arcing or failure: 1. In the radial direction, between the HV electrode and the ground wire and 2. In the axial direction, between both ring electrodes on the outside of the dielectric tube. Therefore, an insulating design and material was chosen to inhibit failure between these locations.

Device components deemed necessary for in vivo plasma medicine devices include a dielectric tube, electrode(s), insulation, and a metallic shield (see Figure 2.1(a)). The insulation design was modeled similar to a coaxial cable, consisting of an inner core (glass tube and electrodes), dielectric insulation, a metallic shield, and an outer shell. The coaxial design theoretically confines the electric and magnetic fields inside the device, allowing safe operation of the device next to surgical instruments with minimal influence. The size and spacing of electrodes selected were within the range found in literature. Potting epoxy with a high dielectric strength provides electrical and thermal insulation to encapsulate electrodes and electrical wires. The outer shell provides structural support, serves as a cavity to hold the potting epoxy and metallic shield, functions as part of the hinge joint to control the bending angle of the tip, and also provides channels to route the tendons. A grounded metallic shield is necessary to ensure there is no electric field outside the walls of device and to prevent any unwanted breakdown/discharges (McKinney, Feasibility Study of In Vivo Robotic Plasma Medicine Devices, International Symposium on Medical Robotics)

2.1.2 Design Requirements

The design goal was to find a compromise between a device that is miniature in size and capable of delivering a plasma plume through a moving tip, while focusing on overall device

safety. There were several key design objectives and requirements considered when designing in vivo plasma medicine devices. Design requirements for the goal are categorized into three categories as listed (McKinney, Feasibility Study of In Vivo Robotic Plasma Medicine Devices, International Symposium on Medical Robotics) © 2019 IEEE.

- Physical requirements: The outer diameter of the device should be minimized for minimally invasive treatment. The maximum device size outer diameter (OD) must be less than 25 mm in diameter, which is the upper limit for current surgical robotic arms such as the da Vinci SP [31]. The inner diameter (ID) of the device should be larger than 3 mm to help treat larger tumors (areas) if necessary. The device must be longer than 200 mm to reach deep-seated organs.

- Safety-relevant functional requirements: For in vivo use, the device is required to be electrically and thermally safe as well as biocompatible. The device must be electrically insulated to seal electrical components from any contact with the human body and to prevent electrical shock. The electric field outside the device must be less than 1 kV/mm to reduce the risk of unwanted breakdown outside the device walls. Unacceptable electrical failures include arcing, material breakdown, and undesirable discharges. Therefore, the operating voltage of the device must be much less than the breakdown voltage. The device must be thermally insulated to have an exterior surface temperature less than 40^{o}C, which is the upper temperature limit allowed inside the human body without causing thermal tissue damage [18].

- Treatment-relevant functional requirement: The device must generate and deliver a stable plasma plume from the dynamically moving, steerable tip, which is crucial in selectively treating target tumors by being able to precisely control plume size and treatment dose.

2.2 Materials and Prototyping

2.2.1 Materials and Dimensions

An atmospheric pressure plasma jet (APPJ), specifically a dielectric barrier discharge (DBD) jet with two ring electrodes was used for all experimental testing. A borosilicate glass tube that

was 6.35 mm in outer diameter and 4 mm in inner diameter was employed as the dielectric tube. The size and spacing of the copper ring electrodes were 5 mm and 15 mm, respectively. The outer cylindrical shells, wire guides, and proximal and distal outer shell sections for the full-scale prototype were 3D printed using a transparent resin (RS-F2-GPCL-04, Formlabs, Somerville, MA, USA), enabling visual investigation of insulation failures during testing. The outer shell had a wall thickness of 1.25 mm for all devices. Two-part potting and encapsulating epoxy (832 C, MG Chemicals, Surrey, B.C., Canada) was used as the insulation material due to its electric insulating properties for high voltage applications (high dielectric strength 15.7 kV/mm @ 3.175 mm) and thermal insulating properties (low thermal conductivity 0.28 W/(m·K) @ 25^{o}C). The low mixed viscosity of the epoxy compound allows it to penetrate small gaps and cavities, necessary to eliminate air pockets [32]. Different insulation thicknesses used in testing were defined by the distance between the outside of the glass tube and the ground shield. Aluminum foil shielding, 0.07 mm in thickness, was used as the grounded metallic shield (McKinney, Feasibility Study of In Vivo Robotic Plasma Medicine Devices, International Symposium on Medical Robotics) © 2019 IEEE.

The 3 different plasma jet devices with insulation thicknesses of 3.5 mm, 4.5 mm, and 5.5 mm, corresponded to outer device diameters of 16, 18, and 20 mm. For devices used in insulation and temperature testing, the lengths of the glass tubes and outer shells were 75 mm and 50 mm, respectively. The ground electrode was positioned 10 mm from the tube exit. A schematic of an insulated plasma device is shown in Figure 2.1(a) (McKinney, Feasibility Study of In Vivo Robotic Plasma Medicine Devices, International Symposium on Medical Robotics) © 2019 IEEE.

On the other hand, for the full-size device, the lengths of the glass tube and outer shell for the proximal and distal sections were 244 mm and 15.09 mm and 210 mm and 14.33 mm, respectively. The proximal and distal glass sections were separated by a gap of 5 mm to allow for bending motion and implementation of an outer hinge joint. Flexible silicone rubber tubing functioned as a bendable joint while connecting the proximal and distal glass sections (McKinney, Feasibility Study of In Vivo Robotic Plasma Medicine Devices, International Symposium on Medical Robotics) ©

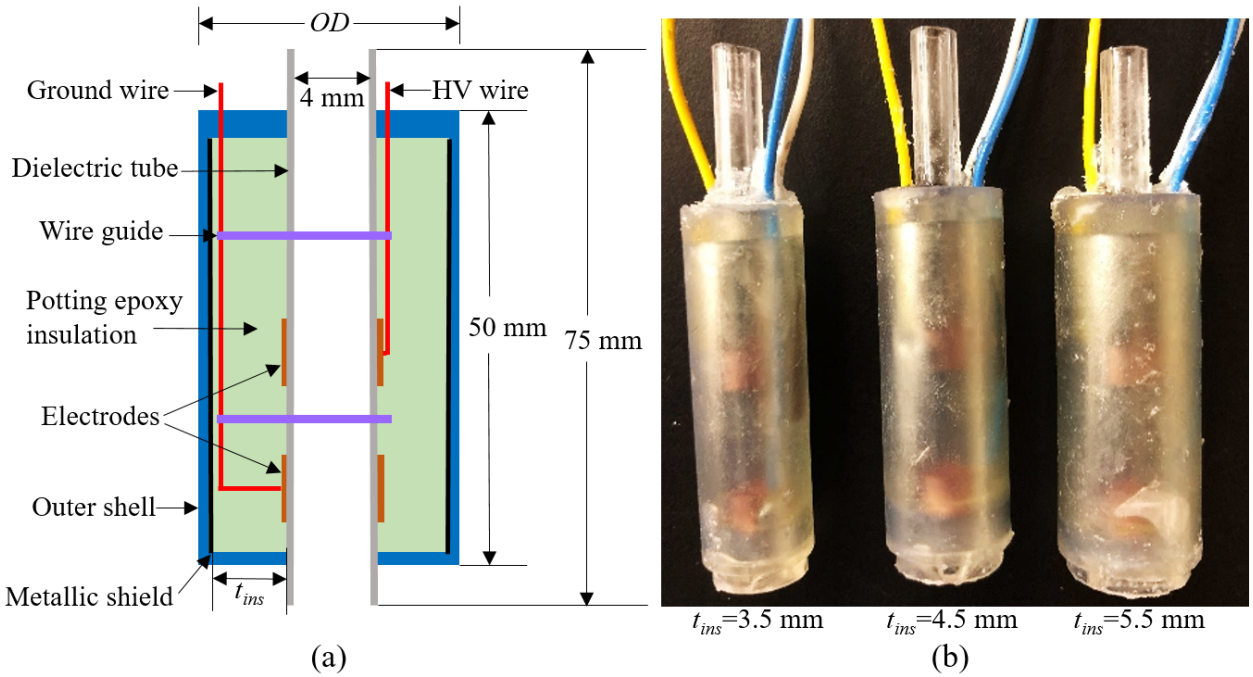

Figure 2.1: (a) Schematic of insulated plasma device used for insulation and temperature testing and (b) Manufactured devices of 3 different insulation thicknesses used for insulation and temperature testing. Reprinted from [7] © 2019 IEEE.

2019 IEEE. A silicone rubber tube with an inner diameter, outer diameter, and length of 4 mm, 7 mm, and 14.9 mm, respectively was used in attempt to keep the inner cross section as constant as possible. The ground electrode was positioned 26.75 mm for the distal tip exit.

2.2.2 Manufacturing Process

The manufacturing process of all plasma devices in this paper was kept as consistent as possible. Borosilicate glass tubes were cut to the specified lengths. Copper tape was cut and wrapped around the glass tube to function as electrodes. Thin electrical wires (22 gauge, 1.5 mm OD) were soldered to high voltage and ground electrodes. The outer cylindrical shell and wire guides were 3D printed. Using a sliding force fit, wire guides were positioned along the glass tube and used to route electrical wires through. Wire guides were necessary to keep the HV and ground wire on opposing sides of the glass tube, while maximizing the distance between the HV wire and the grounded shield and positioning the ground wire away from the HV electrode. The aluminum foil

shield was placed along the inner walls of the outer shell. The glass tube was inserted inside the outer shell and held concentric by sliding force fits at the device top and bottom. Two-part potting epoxy was mixed slowly and thoroughly and allowed to sit for 15 minutes to de-air. The epoxy was poured into the cavity of the outer shell from the device top to encapsulate the electrodes and electrical wires and allowed to cure at room temperature for at least 24 hours. Precautions were taken in attempt to eliminate any voids in insulation and remove any air bubbles and gaps. Images of 3 different prototyped devices used for insulation and temperature testing are shown in Figure 2.1(b) (McKinney, Feasibility Study of In Vivo Robotic Plasma Medicine Devices, International Symposium on Medical Robotics) © 2019 IEEE.

A few additional steps were required for prototyping of the full-size device. An image of the full-scale plasma device rigged prior to adding insulation is shown in Figure 2.2. The silicone rubber tube was slipped over and bonded to the outside of the glass tubes to connect proximal and distal sections. Thin electrical wires were soldered to electrodes and then connected to continuous-flex insulated wires (18 gauge, 6.35 mm OD) near the inlet of the proximal section using crimp-

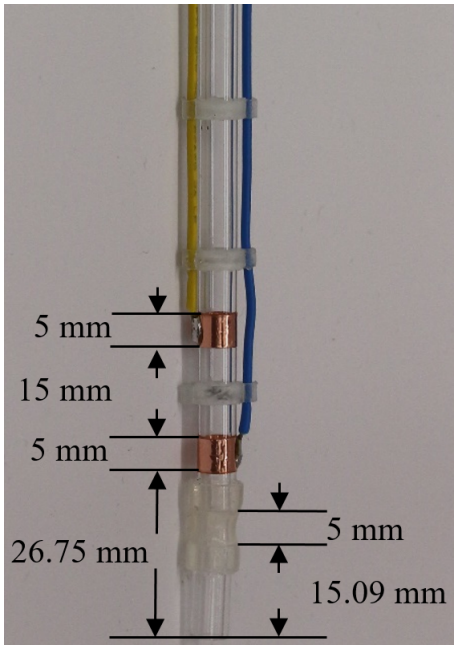

Figure 2.2: Full-scale device rigged with electrodes, wire guides, and electric wires without insulation.

on butt splices. Proximal and distal outer shells with connectable hinge joints were 3D printed. Braid/PTFE composite tubes (1mm OD) were bonded along the top and bottom sides of the outer shell sections to function as dual tendon channels. The aluminum foil shield was inserted inside the proximal shell. The rigged glass device shown in Figure 2.2 was inserted inside the proximal outer shell, and the epoxy insulating process was followed. After the epoxy cured, proximal and distal sections were connected via the hinge joint. Pins were inserted into the hinge joint, constraining the proximal to the distal section, and preventing any movement of the distal section in the axial direction. Vision markers were glued to platforms on the proximal and distal sections for joint angle estimation. Kevlar tendons, 0.21 mm in diameter, were routed through tendon channel tubes and connected to the robotic controller. A schematic and images of the full-scale robotic plasma device connected to the robotic interface are shown in Figure 1.4 and Figure 2.3.

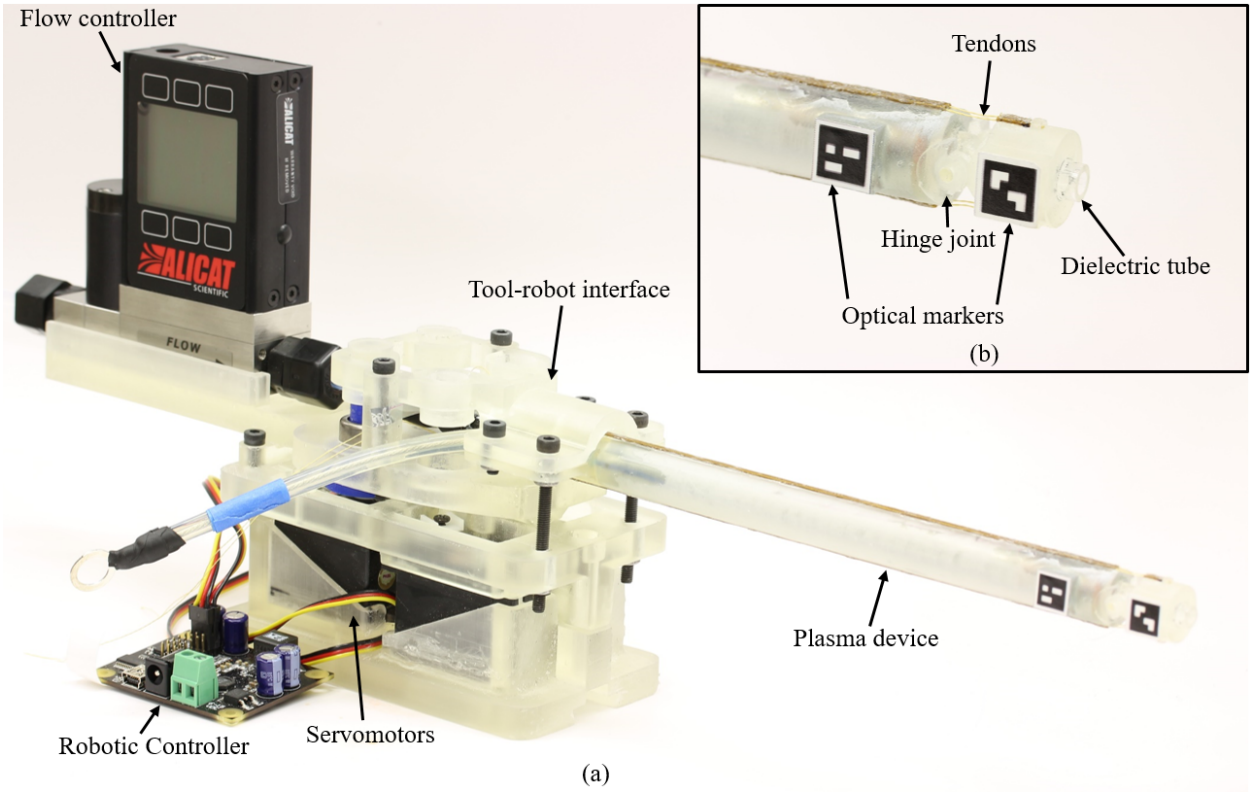

Figure 2.3: (a) Image of robotic plasma device depicting major components of robotic system and (b) Image of tip portion of device highlighting critical device components.

Robotic system components including the servomotor enclosure box and tool-robot interface were 3D printed. The proximal outer shell of the device was mounted to the robotic interface using M4 bolts and nuts. The single degree of freedom, robotic plasma device was tendon actuated using servomotors and had a distal tip range of motion of $\pm 41^{o}$.

2.3 Failure Modes and Effects Analysis

Failure modes and effects analysis was conducted to identify potential problems of the robotic plasma medicine device system and their impact to help mitigate failures. This risk assessment is necessary to examine the safety and reliability of the proposed device during operation. The failure modes of all equipment including the plasma device, robotic system, flow controller, and power supply were addressed. The scoring system of each category was adopted from [33]. The scoring system used, including scale and description, is shown in Table A.1 of Appendix A.

One possible failure mode is for the device to fail to generate plasma. This failure mode could be due to electrical wires becoming disconnected from the electrodes, the ground source, or the power supply, or the grounded metallic shield being in common contact with the high voltage electrode. To help prevent this, wires were soldered to electrodes, and electrical wires were securely connected to high voltage and ground sources. The second failure mode identified is the plasma device leaking gas. A chipped or broken glass tube, a faulty connection between flexible tubing and glass tube, and disconnection of the flexible tube joint are possible sources of this failure mode. Therefore, a sealed and bonded connection between flexible and glass tubing was used. The third failure mode identified is insulation breakdown inside the device. Inconsistent mixing of epoxy, air bubbles, and voids in insulation can lead to premature device failure. Insulation breakdown would be rather catastrophic and yield a destroyed, unusable device. The possibility of this failure mode was alleviated by thoroughly mixing the correct epoxy compound ratio and eliminating air bubbles using a de-airing process prior to pouring the epoxy inside the device cavity. The fourth failure mode is external discharges surrounding the device and possible electrical shock. This could be caused by the metallic shield not being grounded or the thin high voltage wire being in close proximity to conductive objects outside the device. External discharges or electric shock

could arise if surrounding gases, conductive tools, or human contact were introduced to the device's electric field. This would be unacceptable and catastrophic inside the body. This failure mode was mitigated by grounding the outer metallic shield, which confines the electric field and any breakdown to inside the device and also adding an insulated high voltage wire outside the device. The fifth failure mode is high device temperature exceeding 40°C. Undetectable voids in insulation causing unwanted partial discharges can result in a rapid increase in device temperature in an unpredictable manner. The sixth and seventh failure modes identified are inability to control tip motion with the device or the robotic system. This could be due to the outer shell joint becoming structurally damaged, a tendon breaking, tendon routing tubes becoming unattached, or a tendon loosening or becoming detached from a servomotor. The seventh failure mode is unstable connection or detachment between the device and tool-robot interface. Making sure all bolts and nuts were tight ensured a secure connection between device and interface during operation. If the gas mass flow controller were to leak, this could cause another failure mode. Faulty or unsecure connections could cause helium gas to leak, potentially becoming harmful after an extended period of time and also resulting in an unknown flow rate downstream of the flow controller. This failure mode was mitigated by ensuring tight, sealed connections between flexible tubing, connectors, and the flow controller. The ninth failure mode recognized is the gas mass flow controller outputting an inaccurate flow rate. This could be caused by improper calibration or contaminates in the gas flow and result in inability to precisely control the plasma dosage. Preventive actions taken to ensure an accurate flow rate include a leak proof flow loop assembly, high accuracy calibration, and verification of the correct flow rate value using a flow meter located far downstream from the flow controller. The final failure mode is the unexpected shut-off of the high voltage power supply, which would prevent plasma generation. Potential causes of this failure mode include a faulty connection to a power source outlet or a blown fuse. The power supply's power cord was securely connected to a working power source outlet to ensure reliable operation. Each failure mode and the accompanying severity, occurrence, detection, and risk priority number (RPN) can be seen in Table 2.1. The failure modes with high risk priority numbers highlight key areas where correcting

actions can be focused, and they require careful analysis to ensure failure does not occur. Insulation breakdown and high device temperature failure modes possess the highest RPN values of 600 and 700, respectively. This is because small voids inside the insulation can be difficult to detect, and insulation breakdown can occur instantaneously, without warning. Voids with discharges can also cause internal heating, shortening the working time for the device to operate safely inside the body, and lead to thermal tissue damage. These problem can be mitigated by following a consistent insulating process. The epoxy insulation (low viscosity, high dielectric strength, low thermal conductivity) must be mixed to homogeneous consistency and fully encapsulate the high voltage electrical components. Vacuum inject molding should be considered to ensure the elimination of all air bubbles.

Table 2.1: Table of failure modes for robotic plasma device system.

Equipment Type	**Failure Mode**	**Severity**	**Occurrence**	**Detection**	**RPN**
Plasma device	No plasma generation	8	2	1	16
	External gas leakage	9	4	3	108
	Insulation breakdown	10	6	10	600
	External discharge/electrical shock	10	3	10	300
	High device temperature	10	7	10	700
	Tip motion control	7	4	3	84
Robotic system	Tip motion control	7	2	2	28
	Unstable connection	6	2	2	24
Flow controller	Inaccurate output flow rate	9	2	6	108
	External gas leakage	9	4	3	108
Power supply	Fails on, fails off	8	2	1	16

3. EXPERIMENTAL METHODS

3.1 Experimental Setup

Experimental testing was performed using a helium gas cylinder, a gas mass flow controller, flexible tubing, an AC high voltage power supply (PVM500-2500 Amazing 1 Plasma Power Generator), a LeCroy 204MXi oscilloscope, a North Star 1000:1 110 MHz high voltage probe, a 4K webcam, a computer, insulated plasma jet devices, and a fume extractor enclosure. Figure 3.1 depicts the schematic of the experimental setup used to perform the insulation testing. A similar setup was used to perform temperature testing and robotic full-scale device testing. Insulated plasma devices used for insulation and temperature testing are shown in Figure 2.1.

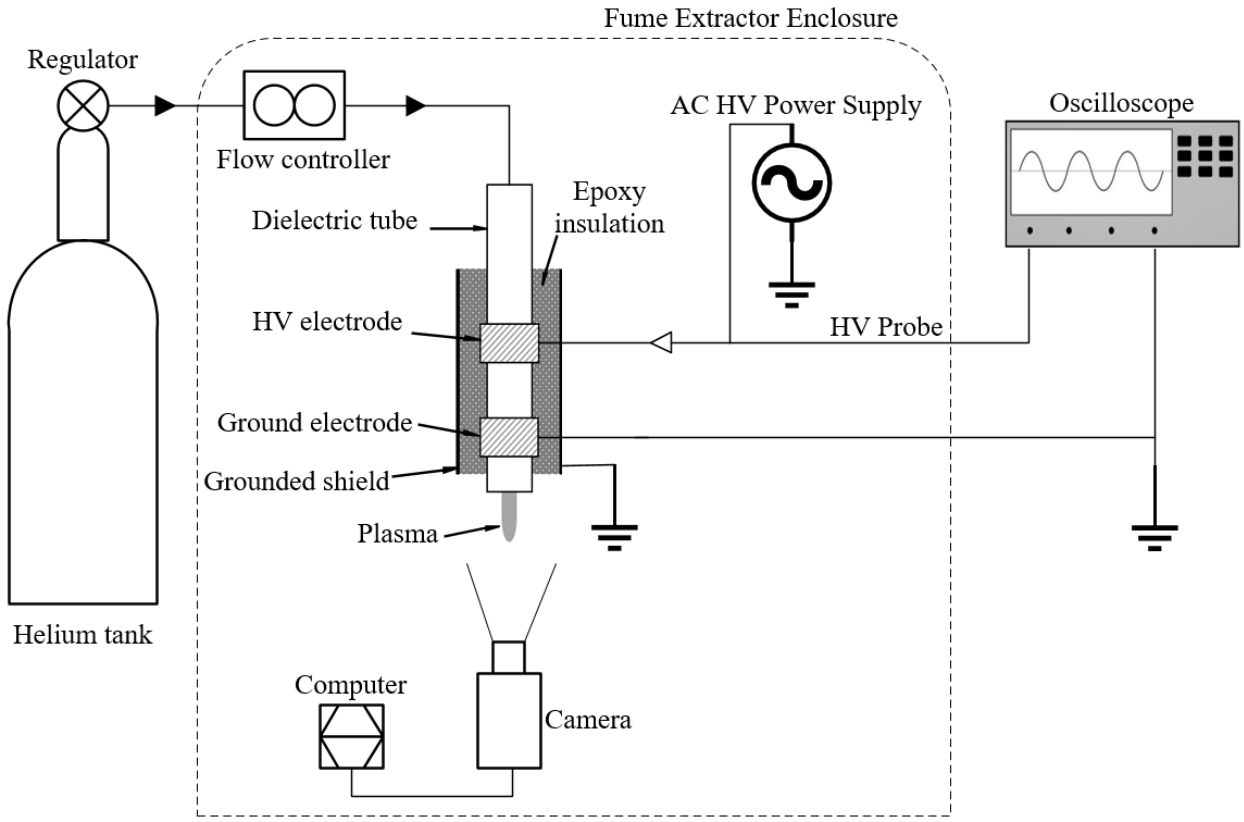

Figure 3.1: Schematic of experimental setup. Reprinted from [7] © 2019 IEEE.

3.2 Insulation Testing

The purpose of this experiment was to determine the effect of insulation thickness and applied voltage on the breakdown voltage and failure of a DBD plasma jet device with 2 ring electrodes and a grounded outer shield.

Prior to insulation testing, a simulation study using COMSOL Multiphysics v5.4 was performed to evaluate the electric field across the insulation and surrounding the HV electrode. The electrode size and spacing, dielectric tube diameter, shield thickness, and dielectric material properties were consistent with manufactured devices. The numerical results showed that the electric field was reduced to zero at the ground shield. However, a high, localized electric field was present at the corner edge of the HV electrode (33.1 kV/mm at 6 kV AC peak voltage and 66.2 kV at 12 kV AC peak voltage), much higher than the dielectric strength of the potting epoxy insulation. This presented the need for further investigation using experimental breakdown testing.

A Test to Breakdown, Step-by-Step test was used to determine the breakdown voltage for different insulation thicknesses. The manner in which insulation testing was conducted is similar to high potential (hi-pot) testing of insulation or cables for high voltage applications in industry [34]. The safety purpose of this test was to identify when and where the device fails, identify the consequences of device failure, and determine an acceptable operating voltage range. The three different insulation thicknesses used for testing include 3.5 mm, 4.5 mm, and 5.5 mm. Three devices were built and tested for each insulation thickness.

Prior to starting each device test, a plasma device was secured vertically by a 3-prong clamp. The high voltage electrode was connected to the power supply's HV power line, and the ground electrode and outer metallic shield were connected to grounded wires. The high voltage probe connected to the oscilloscope was also attached to a small exposed section of the high voltage wire in order to measure applied voltages. A 4K webcam was mounted in front of the plasma device to record video of the device during plasma generation and failure. All videos were recorded in 4K resolution at 30 frames per second.

The helium gas cylinder was opened, and the gas mass flow controller was set to 3 SLPM

to control the helium gas flow rate into the plasma jet device. The power supply was turned on, and the frequency was set to 20 kHz with sinusoidal waveform for discharge generation. The independent voltage level control knob was slowly increased to 50% (about 7.5 kV peak voltage), where the device generated a plasma jet for 1 minute. The independent voltage level control knob was increased by 10% after every 1 minute of operation, until visible failure occurred. Peak voltage readings displayed by the oscilloscope were recorded at each voltage step, including at breakdown. After device failure, the independent voltage level control knob was decreased back to zero, and the power supply was turned off. The gas flow regulator was also turned to close off gas flow. The incremental voltage and breakdown measurement steps were repeated for 9 total devices, 3 of each insulation thickness (McKinney, Feasibility Study of In Vivo Robotic Plasma Medicine Devices, International Symposium on Medical Robotics)

For post processing, each device and video was examined to investigate origin of breakdown and failure modes. An axial cut was made down each device, and the external resin shell and metallic shield were peeled off to inspect the internal components. Video footage of each device during breakdown was also analyzed in slow motion.

3.3 Temperature Testing

The objective of this experiment was to determine the effect of insulation thickness on the device outer surface temperature of a DBD plasma jet device with 2 ring electrodes and a grounded outer shield. Temperature testing was important to study the heat transfer through the insulation and to determine the device outer shell temperature increase over time during plasma generation at a set applied voltage. The three different insulation thicknesses used for temperature testing include 3.5 mm, 4.5 mm, and 5.5 mm. One device was build and tested for each insulation thickness.

A fiber-Bragg-gratings (FBG) sensor that is insensitive to an electromagnetic field was selected for temperature measurement. Prior to beginning temperature testing, the optical fiber sensor was calibrated. With a K-type thermocouple ($\pm 1^{o}$C accuracy, 1 second time/sample interval) and a FBG optical fiber sensor secured inside a metal pot in an unstrained position, hot water at 60^{o}C was poured into the pot and allowed to cool until nearly room temperature. A calibration curve

was generated to determine the relationship between wavelength data of the FBG sensor and temperature data of the thermocouple as presented in Figure 3.2.

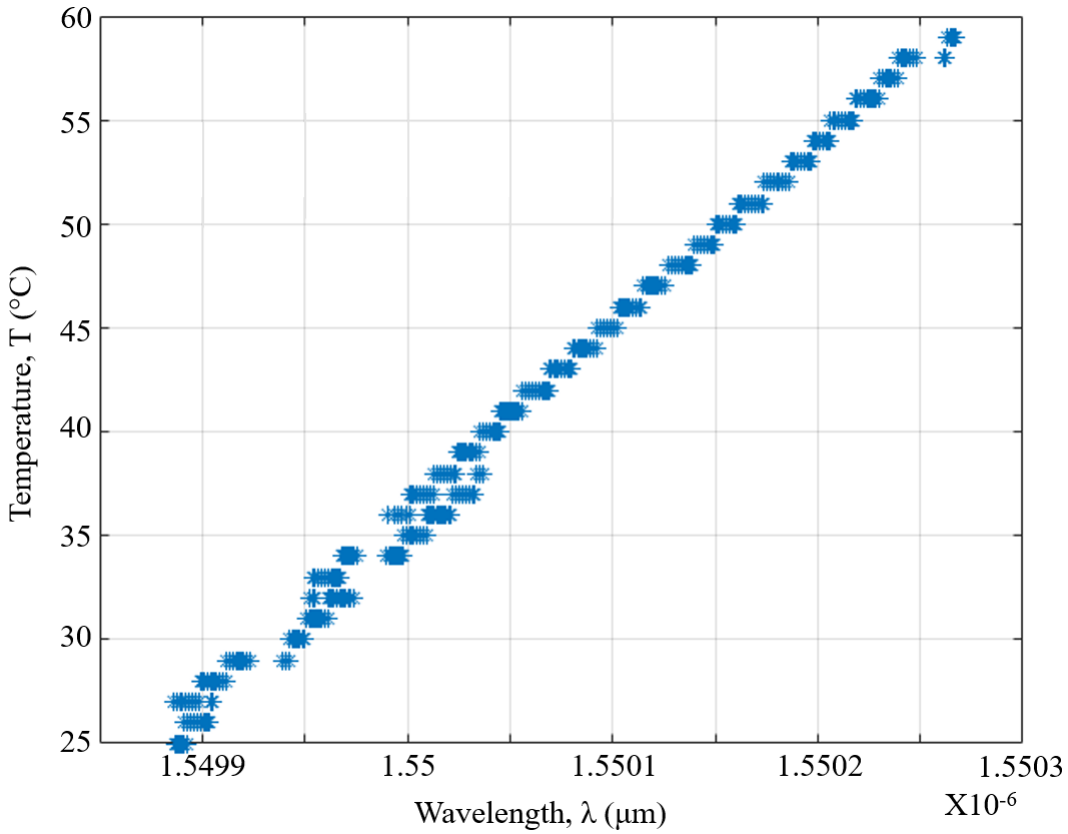

Figure 3.2: Calibration curve showing linear relationship between wavelength and temperature.

For experimental testing, the FBG optical fiber sensor, approximately 8 mm in length, was secured in an unstrained position and in the axial direction on the outer shell surface by applying Scotch tape on both sides of the sensor. The optical fiber was connected to the optical sensing interrogator, which was connected to a power supply and computer. With helium gas flow on, the independent voltage level control knob of the power supply was set to 30% (about 4.5 kV peak voltage). The device generated a plasma jet for 8 minutes, and the wavelength data of the FBG sensor was recorded at 100 Hz (McKinney, Feasibility Study of In Vivo Robotic Plasma Medicine Devices, International Symposium on Medical Robotics) © 2019 IEEE. These temperature mea-

surement steps were repeated for 3 total devices, 1 of each insulation thickness. Post processing of the recorded data included converting the wavelength measurements to temperature using the calibration function.

3.4 Robotic Full-Scale Device Testing

The objective of this experiment was to investigate the feasibility of delivering a plasma plume through the moving distal tip of a DBD plasma jet device with 2 ring electrodes and a grounded outer shield. A single, full-scale device with an insulation thickness of 3.5 mm was built and tested (McKinney, Feasibility Study of In Vivo Robotic Plasma Medicine Devices, International Symposium on Medical Robotics) © 2019 IEEE. This insulation thickness was selected to help minimize the device outer diameter for minimally invasiveness.

The robotic controller interface system consisting of a robotic controller, servomotors, roller bearings, and tool-robot interface was assembled. The proximal section of the plasma jet device was mechanically secured to the robotic interface, which is compatible with the current dA Vinci EndoWrist arm (Intuitive Surgical Inc., Sunnyvale, CA) (McKinney, Feasibility Study of In Vivo Robotic Plasma Medicine Devices, International Symposium on Medical Robotics) © 2019 IEEE. The Kevlar tendons were connected to two servomotors, which were controlled by a robotic controller connected to a computer. An image of the single degree of freedom, full-scale robotic plasma device connected to the robotic interface is shown in Figure 2.3.

The distance between the distal tip exit and the grounded aluminum plate substrate at a 0^{o} tip angle was set at 15 mm. With helium gas flow on, the independent voltage level control knob of the power supply was set to 25% (about 3.75 kV peak voltage). The bending of the tip was controlled through tendon actuation (McKinney, Feasibility Study of In Vivo Robotic Plasma Medicine Devices, International Symposium on Medical Robotics) © 2019 IEEE. Real-time tip angle estimation was determined using optical marker joint angle estimation and a 4K webcam. A DSLR camera was used to record video of the plasma plume being delivered through the moving tip over a range of motion from -30^{o} to 30^{o}.

3.5 Electrical Diagnostics of Dielectric Barrier Discharge

The proposed device in this thesis is a dielectric barrier discharge plasma jet device consisting of two ring electrodes around a borosilicate glass tube and encapsulated in epoxy insulation. For DBDs, the measurements of voltage and current data during device operation as well as parameters of the plasma are influenced by discharge geometry. Knowledge about the dissipated energy and power and voltage and current in the gas gap is necessary for characterization, comparability, and scaling of DBDs [35]. Thus, interpretation of discharge characteristics and quantities can provide useful insight into the plasma behavior of a specific DBD prototype.

DBD reactors consist of three main parts: conductive electrodes where voltage, current, and charge can be measured; dielectric barriers that inhibit the flow of conducted current through the reactor; and the gas gap where gas/plasma discharge occurs (see Figure 3.3(a)). The equivalent diagnostics of the DBD involves using an equivalent circuit approach as described in [36], from which measured voltage and current waveforms can be used to infer information about a DBD's discharge properties. A diagram of the equivalent circuit model is shown in Figure 3.3(b).

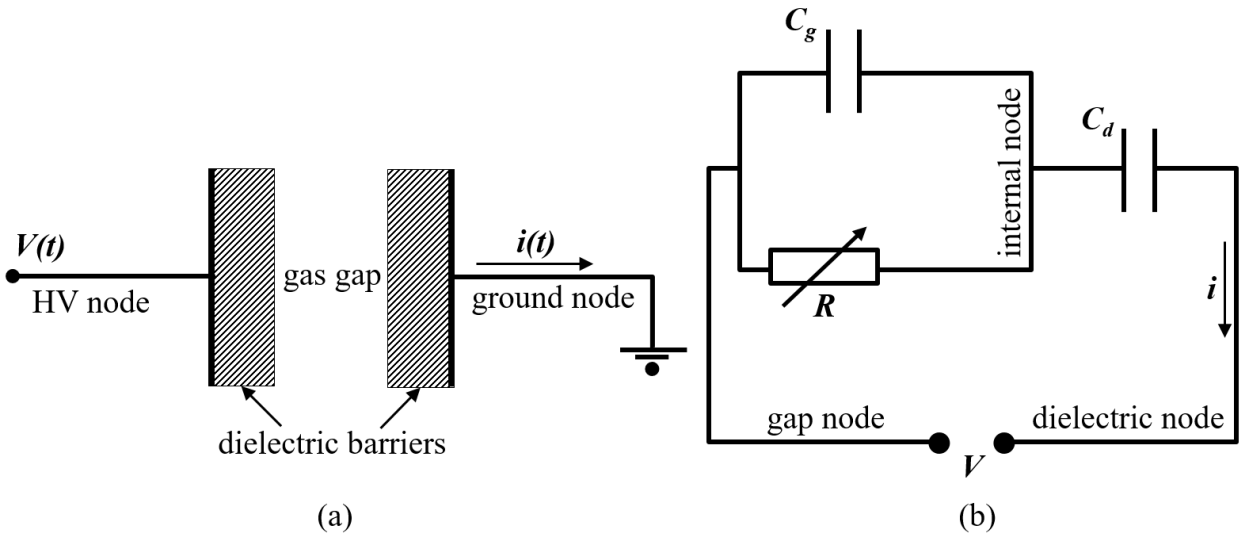

Figure 3.3: (a) Schematic of dielectric barrier discharge cell and (b) Diagram of simplest equivalent circuit model of a DBD.

An ideal or classical charge-voltage plot, also known as a Lissajous figure, has a parallelogram shape with distinguishable discharging phases, as shown in Figure 3.4. Parameters such as the reactor cell capacitance, C_{cell}, dielectric barrier capacitance, C_d, breakdown voltage, U_b, total plasma energy per cycle, and total power per cycle can be deduced from the parallelogram.

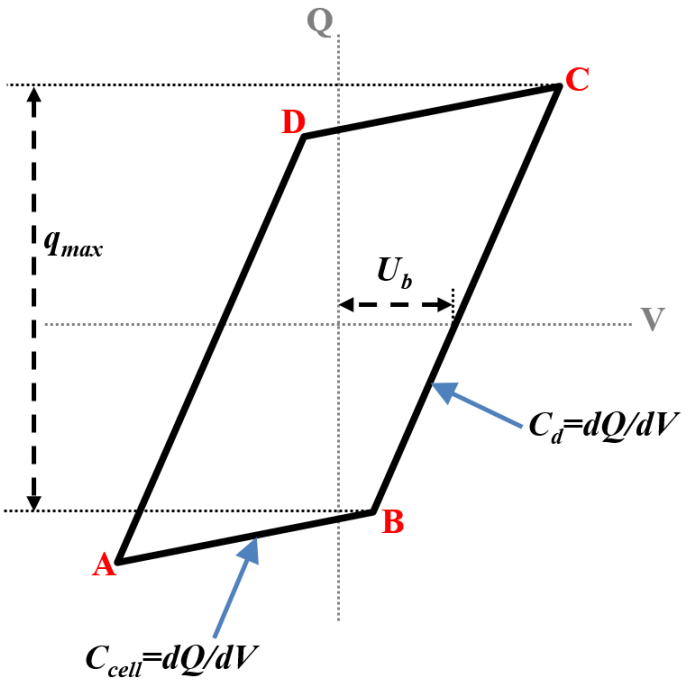

Figure 3.4: Schematic of classical charge-voltage Lissajous plot.

According to DBD capacitance alternation, the capacitance of the DBD reactor is governed only by the capacitance of the dielectric barriers, C_d, when the discharge channel fills the gas gap. However, when discharge in not present, the DBD capacitance is significantly smaller and equal to the cell capacitance, C_{cell}. The slopes (dQ/dV) of sides B-C and A-B indicate two values of effective discharge capacitance, C_d and C_{cell}, respectively. C_{cell} can also be calculated as a connection of gas gap and dielectric barrier capacitances in series:

$$C_{cell} = \frac{C_d C_g}{C_d + C_g} \tag{3.1}$$

Since reactor cell and dielectric barrier capacitances can be directly determined from the Lissajous curve, Eq. 3.1 can be used to calculate the gas gap capacitance, C_g. In the active discharge phase (plasma on) corresponding to sides B-C and D-A, the gas gap voltage remains constant and equal to the effective breakdown voltage, U_b, the voltage at which charge transfer through the gas gap begins. The dark phase (plasma off) corresponds to sides A-B and C-D in the parallelogram. The charge difference between points B and C, a variation of measured charge during the active discharge phase, is the maximum charge transferred through the gas gap, q_{max}. The area inside the Q-V curve represents the energy dissipated per cycle, from which the power consumption per cycle can be determined by dividing by time per cycle.

During experimental insulation testing, the oscilloscope, HV probe, and a current transformer were used to record voltage and current data of a DBD prototype with an insulation thickness of 3.5 mm at 10.72 kV AC peak voltage. Electrical diagnostics were performed on the DBD device using the Lissajous analysis method.

4. RESULTS AND DISCUSSION

4.1 Insulation Testing

The average breakdown voltages and respective standard deviations of the tested devices with 3.5 mm, 4.5 mm, and 5.5 mm of insulation thickness were 11.63 kV $\pm$ 0.12 kV, 11.7 kV $\pm$ 0.56 kV, and 12.85 kV $\pm$ 0.92 kV, respectively. Breakdown voltage increased with insulation thickness.

The order in which breakdown occurred for a device with 3.5 mm of insulation thickness is shown by a sequential set of images displayed in Figure 4.1(a). Breakdown initiated at the top edge of the high voltage electrode, expanded radially to the ground wire or grounded shield, and subsequently propagated axially along the glass tube to the grounded electrode. Physical inspection of the devices post testing revealed the locations where failure occurred evident by black burn marks or carbonized tracking and treeing of the insulation. Figure 4.1(b) shows the visible failure of a device with an insulation thickness of 3.5 mm after removal of the outer shell and shield (McKinney, Feasibility Study of In Vivo Robotic Plasma Medicine Devices, International Symposium on Medical Robotics) © 2019 IEEE.

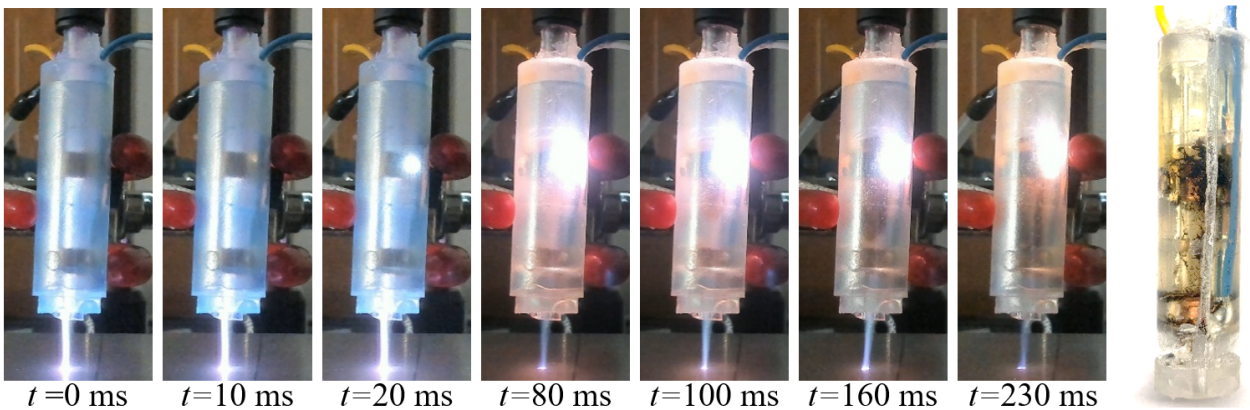

Figure 4.1: (a) Sequence of failure for device with 3.5 mm of insulation thickness at 11.7 kV and (b) Post testing image of that dissected device showing tracking of internal failure. Reprinted from [7] © 2019 IEEE.

All devices tested, independent of insulation thickness, failed at relatively high voltages (11.1 kV to 13.5 kV) and exhibited similar failure modes. From this result, it can be assumed that the manufacturing of devices, including mixing and potting of epoxy, was done in a consistent manner. However, only 2 of the 3 devices with an insulation thickness of 5.5 mm were tested due to one device with a fault in manufacturing in which the ground shield was in common contact with the HV electrode. Post testing, physical device dissection and video review allowed for a more in depth diagnosis and analysis of failure. Examination of the slow motion videos during testing showed that failure first occurred radially and then axially to the ground electrode, as illustrated in Figure 4.1(a). Since failure occurred in the radial direction first, at this electrode spacing, breakdown was dependent on the insulation thickness. Some videos were difficult to analyze due to a large instantaneous flash present during breakdown. Therefore, only some devices were able to be clearly analyzed via video. Although failure was confined inside the device by the grounded shield, it can be assumed that any breakdown during in vivo treatment would be unacceptable and could be catastrophic. Therefore, it should be noted that all devices and insulation thicknesses tested yield a safety factor, defined as breakdown voltage divided by operating voltage, of 1.48 or greater for an operating voltage of 7.5 kV (McKinney, Feasibility Study of In Vivo Robotic Plasma Medicine Devices, International Symposium on Medical Robotics) © 2019 IEEE. It is worth mentioning that the 3-prong metal clamp used to hold the devices during testing could have possibly contributed to device breakdown.

A few limitations of the experimental insulation breakdown testing can be noted. Although the power supply's independent voltage level control knob was increased by 10% after every minute of operation, the voltage step increments were not the same for all devices or insulation thicknesses. In addition, the HV probe from the oscilloscope had a noticeable effect on plasma generation, in which devices were only able to generate a visible plasma plume at the minimum frequency setting on the AC HV power supply (20 kHz).

4.2 Temperature Testing

A plot of the device outer shell surface temperature over the first 100 seconds of operating time for the 3 different devices used to perform temperature testing is shown in Figure 4.2. The initial surface temperature in room temperature conditions of all 3 devices prior to plasma generation was around 25°C. The devices with 3.5 mm and 4.5 mm of insulation failed internally at 189 seconds and 280 seconds of plasma generation, respectively, in which maximum surface temperatures of 86°C and 85°C, respectively were reached. On the other hand, the device with an insulation thickness of 5.5 mm reached its highest surface temperature of 90°C after 480 seconds of operation, without any noticeable failure. The rate of temperature increase decreased with an increase in insulation thickness. The main interest of temperature testing was to determine the duration for the devices to reach 40°C, the temperature limit before possible thermal tissue damage. The operating time for the outer shell temperature to reach 40°C was 42 seconds, 78 seconds, and 84 seconds for 3.5 mm, 4.5 mm, and 5.5 mm of insulation, respectively.

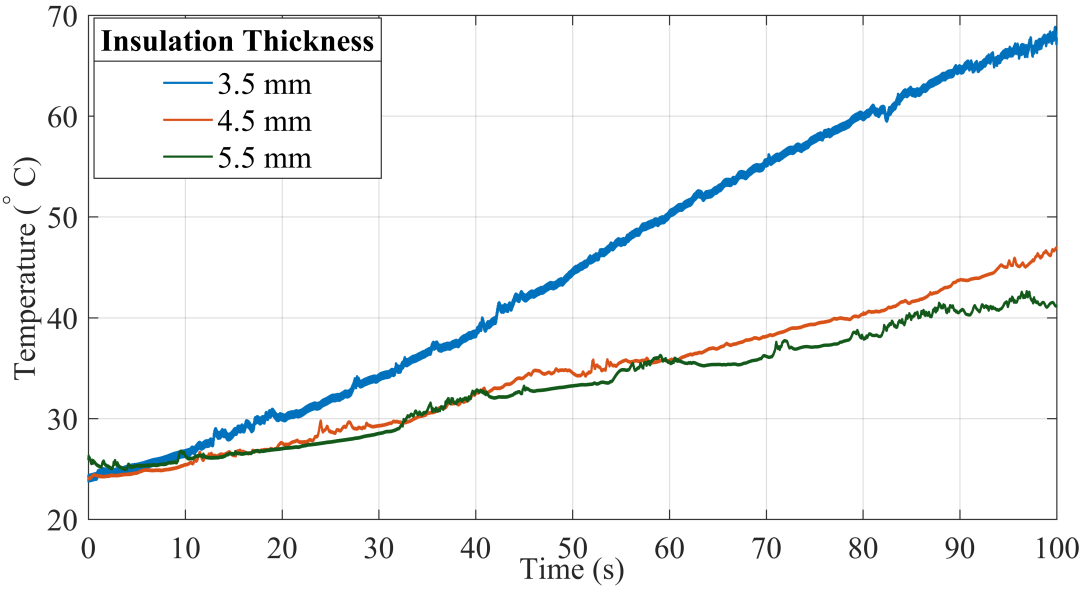

Figure 4.2: Plot of device outer shell temperature measured by FBG sensor over time for 3 devices with different insulation thicknesses. Adapted from [7] © 2019 IEEE.

A specific operating time limit of the plasma devices would be necessary for use inside the human body to ensure the device temperature does not exceed 40°C. These devices would likely only be safe to generate plasma in vivo for a minute or less, depending on insulation thickness and voltage (McKinney, Feasibility Study of In Vivo Robotic Plasma Medicine Devices, International Symposium on Medical Robotics) © 2019 IEEE. Possible sources of breakdown for the devices that failed during temperature testing include voids in insulation around the HV electrode or HV wire, air pockets, and thermal expansion of the epoxy insulation.

Temperature increase of the device is due to a combination of heating effects including joule heating, in which the current passing through the powered electrode and energy from the electric field produces thermal energy and also radio frequency (RF) heating, also known as dielectric heating, in which a radio frequency alternating electric field heats the dielectric material. It is important to mention that the first set of devices manufactured for temperature testing failed almost instantaneously due to an air gap, near the cap between the thin HV and ground wire. From the second set of manufactured devices, two of the three devices failed short of 8 minutes of operating time. Any partial unwanted discharges present inside air bubbles within the insulation that eventually lead to device breakdown is a possible reason for the rapid heating. Possible ways to achieve longer safe device operating times include increasing the insulation thickness, using an insulating material with a lower thermal conductivity, and selecting a different dielectric tube material with a higher dielectric constant so that the device can operate at a lower voltage to achieve the same power.

Possible limitations of the experimental temperature testing method include that the FBG sensor is only as accurate as the thermocouple used to calibrate it (± 1°C accuracy, 1 second time/sample interval), and an air draft in the room could possibly influence readings by inducing a small strain on the optical fiber.

4.3 Robotic Full-Scale Device Testing

The plasma plume being delivered through the distal tip over a range of motion from -30° to 30° is shown in Figure 4.3.

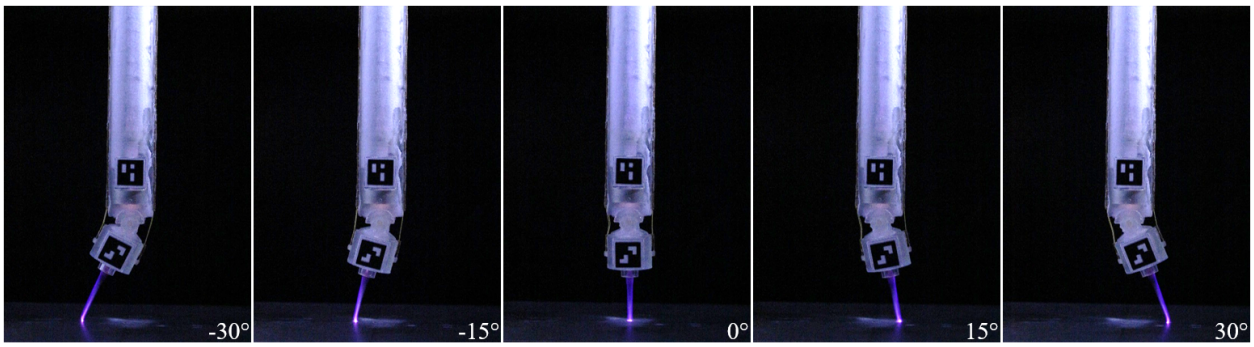

Figure 4.3: Sequence of images over oscillation cycle showing plasma generation through distal tip at various angles.

During motion at higher tip angles (near the extremes $\pm 41^{o}$), the stability of the plasma plume was visibly influenced in which the plume length did not fully extend to the grounded aluminum plate substrate. This problem could be mitigated by decreasing the distance to the substrate (<15 mm) or increasing the gas flow rate (>3 SLPM). Also, the working range of angular tip motion during plasma delivery could be limited from -30^{o} to 30^{o} or less to help minimize the change in working distance.

Limitations of robotic full-scale device experimental testing were that the distal tip could not oscillate in a smooth, continuous motion. When one tendon was in tension and being actuated by a servomotor, the opposing tendon remained in slack. When changing tip directions, one tendon/servomotor was disengaged (put back into slack) while the other tendon took a moment to retract its slack and engage into tension. The slack in the tendons and the servomotors operating at separate times created a slight delay in tip motion. A smooth, more continuous tip motion may be possible if a control algorithm were developed and implemented.

4.4 Electrical Diagnostics of Dielectric Barrier Discharge

The measured voltage and current waveforms for a DBD prototype with an insulation thickness of 3.5 mm are shown in Figure 4.4. The frequency is 19.5 kHz, and the time period per cycle is 5.13 x 10^{-5} s. Peak voltage and current amplitudes are 10.72 kV and 17.3 mA, respectively. The main current pulses or peaks appear in each half cycle of the voltage and represent microdischarges.

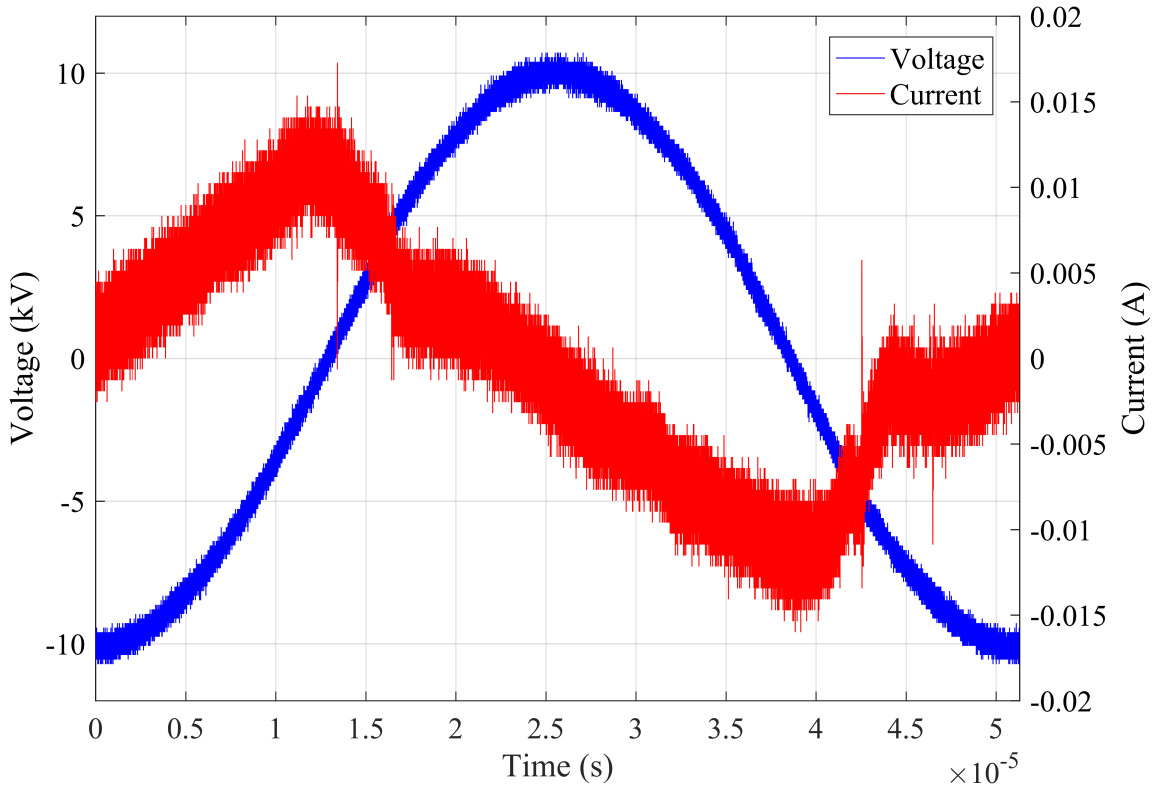

Figure 4.4: Measured voltage and current waveforms of a DBD prototype with 3.5 mm of insulation thickness for 1 cycle.

The current data was integrated over time to determine charge. An experimental Lissajous plot was generated by plotting voltage against charge, as shown in Figure 4.5. The experimental Q-V curve follows a similar shape to the ideal parallelogram, which allows for a more accurate analysis. Linear lines of best fit were applied through each side of the parallelogram to determine their slopes. The total reactor cell capacitance, C_{cell} and dielectric barrier capacitance, C_d were determined to 2.842 pF and 8.252 pF, respectively. The capacitance during the active phase was 2.9 times higher than during the dark phase. The gas gap capacitance, C_g was determined to be 4.334 pF using Eq. 3.1. The effective breakdown voltage of the gas, U_b was 1.766 kV. The maximum charge transferred through the gas gap, q_{max} was 131.2 nC. Plasma energy per cycle and average power per cycle were found to be 5.518 x 10^{-4} J and 10.76 W, respectively.

The proportional and undistorted parallelogram curve may signify some stability during device

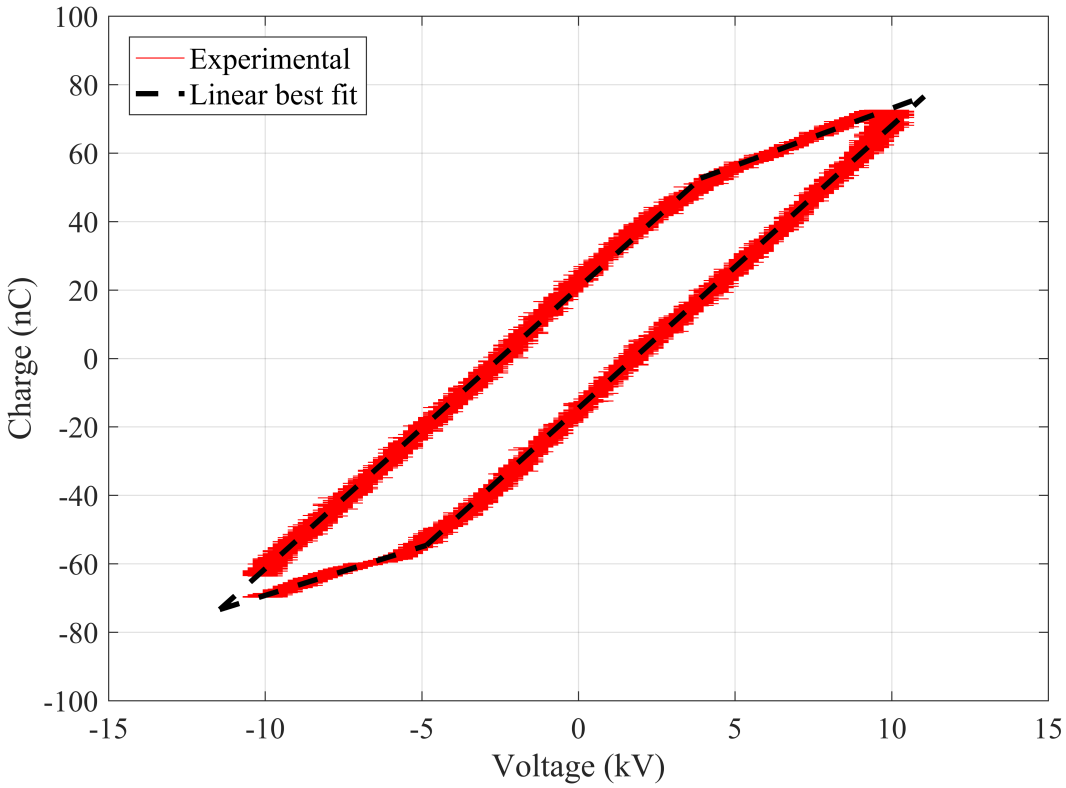

Figure 4.5: Experimental Lissajous figure (Q-V plot) of a DBD prototype for 1 cycle.

operation due to the symmetric electrodes and even discharge gap. Smoothness of right and left sides show stable discharge. The corners of the Lissajous figure represent distinct discharge termination points, whereas round corners can imply possible parasitic resistance than can occur when the barrier material is heated and becomes conductive.

Limitations of using the Lissajous figure as an electrical analysis method for DBDs include that the shape and distortions of the parallelogram can induce variances, making some Q-V plots difficult to accurately analyze. Asymmetric discharge arrangements, uneven discharge gaps, unstable HV power supplies, and measuring elements can be of influence. In addition, the analysis performed was only on on a single, sinusoidal voltage/current cycle. Analysis of many cycles may provide a more accurate analysis, accounting for some fluctuations in current spikes.

5. CONCLUSIONS

This thesis explored the design and feasibility of a robotic plasma medicine device intended for cancer treatment inside the human body, potentially enabling the delivery of cold atmospheric plasma in a safe, controllable, and minimally invasive manner. A device with design features including a steerable distal tip and safe plasma generation was build, satisfying both physical and functional requirements. The safety of prototypes was investigated experimentally by insulation breakdown and device temperature testing. Sufficient insulation, both electrical and thermal, is imperative for an in vivo plasma medicine device. Since breakdown voltage increased with insulation thickness and failure occurred in the radial direction first, device breakdown was dependent on insulation thickness. For in-body use, the operating voltage would have to be significantly lower than the breakdown voltage values. The rate of device temperature increase decreased with an increase in insulation thickness. The tested devices would only be safe to generate plasma in vivo for about a minute or less before possible thermal tissue damage, depending on insulation thickness and voltage. It was also seen that consistent manufacturing and eliminating any voids in insulation (air gaps) surrounding the high voltage electrode and high voltage wire is essential, as evident by device failures. This robotic plasma device can be used as a foundation for future research: to make improvements and focus on better defining plasma dosage parameters including flow rate, voltage, power, and time, for this specific DBD device.

The design and experimental verification testing performed were used to evaluate the feasibility of the proposed full-scale robotic plasma device according to satisfaction of the design requirements stated in Section 2.1.2. The defined physical requirements were an inner diameter greater than 3 mm, an outer diameter less than 25 mm, and a length greater than 200 mm. All dimensional requirements of the robotic full-scale device were satisfied with an inner diameter, outer diameter, and length of 4 mm, 16 mm, and 229 mm, respectively. The defined safety-relevant requirements were that the device must be biocompatible, electrically safe defined by an electric field less than 1 kV/mm outside the device, and thermally safe defined by an exterior surface temperature less

than 40°C. Breakdown and electric field requirements were satisfied by implementing an outer grounded metallic shield as well as defining the operating voltage range to be much less than the average breakdown voltage of 11.63 kV for 3.5 mm of insulation thickness. The thermal requirement was satisfied by defining the safe operating time to be less 42 sections, before possible thermal tissue damage for an insulation thickness and applied voltage of 3.5 mm and 4.5 kV, respectively. The biocompatiblity of the device will be addressed in the future. The defined treatment-relevant requirements were that the device must generate and deliver a stable plasma plume through the dynamically moving, steerable tip. The full-scale robotic demonstrated a plasma plume successfully delivered through the dynamic tip. Although the placement of the ring electrodes before the steerable joint is believed to help with plasma stability, this treatment requirement has not been confirmed yet. Future work will focus on verifying the stability of the plasma by measuring the energy per cycle at different tip angles throughout the oscillation cycle using the Lissajous analysis. If the energy per cycle is maintained within a small threshold value, this will verify plasma stability during operation of the robotic plasma medicine device and its steerable distal tip.

One possible approach to investigate the effect of plasma dosage parameters on plasma stability and plasma flow distribution is to perform plasma enhanced chemical vapor deposition (PECVD) testing, in which a monomer is introduced into the gas flow, and a thin polymer film is deposited onto a substrate. A design of experiments could be conducted to determine the effect of voltage/power and deposition distance on sample thickness distribution, step height, surface roughness, deposition diameter, deposition rate, and substrate temperature. Assuming a smooth, uniform deposited sample is one way to demonstrate the ability to precisely control and deliver a plasma dose, optimal power and deposition distance parameters determined from static, straight angle testing could be applied for dynamic testing with the moving tip. After the completion of more testing, the design of the robotic plasma device can be further improved to allow multiple degree of freedom tip motion. A biocompatible cover needs to be added around the outside of the device as well as between proximal and distal sections. A control algorithm can be developed to work in conjunction with vision-based joint angle estimation to allow both smooth, oscillatory tip

motion and accurate control of tip angle and angular velocity.

Many steps would be required if this new device were to pursue medical device certification for clinical use in the future. The device would require sound and reputable scientific characterization prior to any medical application. Furthermore, the device would have to be deemed a reliable plasma source and demonstrate its safety through biocompatibility, temperature, and electromagnetic compatibility testing and its effectiveness through in vitro testing and preclinical animal studies. This process including device design, manufacturing procedures, risk assessment, and all testing must be well documented in order to meet FDA regulations for a quality system. Recommended operating parameters and the appropriate plasma dose would also need to be well defined according to the type of cancer being treated.

REFERENCES

[1] M. G. Kong, G. Kroesen, G. Morfill, T. Nosenko, T. Shimizu, J. Van Dijk, and J. Zimmermann, "Plasma medicine: an introductory review," *new Journal of Physics*, vol. 11, no. 11, p. 115012, 2009.

[2] G. Morfill, T. Shimizu, B. Steffes, and H. Schmidt, "Nosocomial infections-a new approach towards preventive medicine using plasmas," *New Journal of Physics*, vol. 11, no. 11, p. 115019, 2009.

[3] K. G. Kostov, M. Machida, and V. Prysiazhnyi, "Generation of cold argon plasma jet at the end of flexible plastic tube," *arXiv preprint arXiv:1411.3976*, 2014.

[4] K. G. Kostov, T. M. Nishime, M. Machida, A. C. Borges, V. Prysiazhnyi, and C. Y. Koga-Ito, "Study of cold atmospheric plasma jet at the end of flexible plastic tube for microbial decontamination," *Plasma Processes and Polymers*, vol. 12, no. 12, pp. 1383–1391, 2015.

[5] M. S. Mann, R. Tiede, K. Gavenis, G. Daeschlein, R. Bussiahn, K.-D. Weltmann, S. Emmert, T. von Woedtke, and R. Ahmed, "Introduction to din-specification 91315 based on the characterization of the plasma jet kinpen® med," *Clinical Plasma Medicine*, vol. 4, no. 2, pp. 35–45, 2016.

[6] "kinpen med," (accessed March 31, 2019). `https://neoplas-tools.eu/en/kinpen-med.html`.

[7] B. McKinney, W. McKinney, S. Pattanshetti, and S. C. Ryu, "Feasibility study of in vivo robotic plasma medicine devices," in *2019 International Symposium on Medical Robotics (ISMR)*, pp. 1–7, IEEE, 2019.

[8] "What is cancer?," (accessed March 31, 2019). `http://www.cancer.gov/about-cancer/understanding/what-is-cancer`.

[9] F. Bray, J. Ferlay, I. Soerjomataram, R. L. Siegel, L. A. Torre, and A. Jemal, "Global cancer statistics 2018: Globocan estimates of incidence and mortality worldwide for 36 cancers in 185 countries," *CA: a cancer journal for clinicians*, vol. 68, no. 6, pp. 394–424, 2018.

[10] "Cancer stat facts: Common cancer sites," (accessed March 31, 2019). `http://seer.cancer.gov/statfacts/html/common.html`.

[11] "Cancer treatments," (accessed March 31, 2019). `https://www.cancerquest.org/patients/treatments`.

[12] "Methods of treatment," (accessed March 31, 2019). `http://www1.udel.edu/chem/C465/senior/fall98/Cancer2/methods.html`.

[13] S. Mohades, "Low temperature plasma for the treatment of epithelial cancer cells," 2017.

[14] D. Staack, "Plasma and their applications," (accessed March 31, 2019). `http://pedl.tamu.edu/index_files/AboutUs.html`.

[15] G. Park, S. Park, M. Choi, I. Koo, J. Byun, J. Hong, J. Sim, G. Collins, and J. Lee, "Atmospheric-pressure plasma sources for biomedical applications," *Plasma Sources Science and Technology*, vol. 21, no. 4, p. 043001, 2012.

[16] K.-D. Weltmann, H.-R. Metelmann, and T. von Woedtke, "Low temperature plasma applications in medicine," *Europhysics News*, vol. 47, no. 5-6, pp. 39–42, 2016.

[17] H. Tanaka, K. Ishikawa, M. Mizuno, S. Toyokuni, H. Kajiyama, F. Kikkawa, H.-R. Metelmann, and M. Hori, "State of the art in medical applications using non-thermal atmospheric pressure plasma," *Reviews of Modern Plasma Physics*, vol. 1, no. 1, p. 3, 2017.

[18] K. Weltmann and T. Von Woedtke, "Plasma medicine-current state of research and medical application," *Plasma Physics and Controlled Fusion*, vol. 59, no. 1, p. 014031, 2016.

[19] J. Liu, R. Wang, H. Yuan, W. Cai, X. Wang, J. Zhang, and J. Fang, "Mri-guided dielectric barrier discharge plasma in vivo: A preliminary study for rectal wall of rabbit," *Plasma Processes and Polymers*, vol. 11, no. 12, pp. 1188–1192, 2014.

[20] M. Keidar, "Plasma for cancer treatment," *Plasma Sources Science and Technology*, vol. 24, no. 3, p. 033001, 2015.

[21] D. Yan, J. H. Sherman, and M. Keidar, "Cold atmospheric plasma, a novel promising anti-cancer treatment modality," *Oncotarget*, vol. 8, no. 9, p. 15977, 2017.

[22] Z. Chen, H. Simonyan, X. Cheng, E. Gjika, L. Lin, J. Canady, J. Sherman, C. Young, and M. Keidar, "A novel micro cold atmospheric plasma device for glioblastoma both in vitro and in vivo," *Cancers*, vol. 9, no. 6, p. 61, 2017.

[23] E. J. Szili, S.-H. Hong, J.-S. Oh, N. Gaur, and R. D. Short, "Tracking the penetration of plasma reactive species in tissue models," *Trends in biotechnology*, vol. 36, no. 6, pp. 594–602, 2018.

[24] S. Mirpour, S. Piroozmand, N. Soleimani, N. J. Faharani, H. Ghomi, H. F. Eskandari, A. M. Sharifi, S. Mirpour, M. Eftekhari, and M. Nikkhah, "Utilizing the micron sized non-thermal atmospheric pressure plasma inside the animal body for the tumor treatment application," *Scientific reports*, vol. 6, p. 29048, 2016.

[25] T.-C. Tsai and D. Staack, "Low-temperature polymer deposition in ambient air using a floating-electrode dielectric barrier discharge jet," *Plasma Processes and Polymers*, vol. 8, no. 6, pp. 523–534, 2011.

[26] M. Polak, J. Winter, U. Schnabel, J. Ehlbeck, and K.-D. Weltmann, "Innovative plasma generation in flexible biopsy channels for inner-tube decontamination and medical applications," *Plasma Processes and Polymers*, vol. 9, no. 1, pp. 67–76, 2012.

[27] S. Reuter, T. von Woedtke, and K.-D. Weltmann, "The kinpen-a review on physics and chemistry of the atmospheric pressure plasma jet and its applications," *Journal of Physics D: Applied Physics*, vol. 51, no. 23, p. 233001, 2018.

[28] S. Bekeschus, A. Schmidt, K.-D. Weltmann, and T. von Woedtke, "The plasma jet kinpen–a powerful tool for wound healing," *Clinical Plasma Medicine*, vol. 4, no. 1, pp. 19–28, 2016.

[29] D. Faircloth, "Technological aspects: High voltage," *arXiv preprint arXiv:1404.0952*, 2014.

[30] E. Csanyi, "7 most known high voltage insulation methods you should know," (accessed March 31, 2019). https://electrical-engineering-portal.com/7-most-known-high-voltage-insulation-methods.

[31] J. Zhao, B. Feng, M.-H. Zheng, and K. Xu, "Surgical robots for spl and notes: a review," *Minimally Invasive Therapy & Allied Technologies*, vol. 24, no. 1, pp. 8–17, 2015.

[32] "Technical data sheet: Translucent epoxy, encapsulating potting compound (832c)," (accessed November 15, 2018). https://www.mgchemicals.com/downloads/tds/tds-832c-2parts.pdf.

[33] "Fmea," (accessed May 20, 2019). http://leansixsigmadefinition.com/glossary/fmea/.

[34] "Ipc-tm-650 test methods manual," (accessed November 15, 2018). https://www.ipc.org/TM/2.5.6.3.pdf.

[35] A. Pipa and R. Brandenburg, "The equivalent circuit approach for the electrical diagnostics of dielectric barrier discharges: The classical theory and recent developments," *Atoms*, vol. 7, p. 14, Jan 2019.

[36] A. Pipa, J. Koskulics, R. Brandenburg, and T. Hoder, "The simplest equivalent circuit of a pulsed dielectric barrier discharge and the determination of the gas gap charge transfer," *Review of Scientific Instruments*, vol. 83, no. 11, p. 115112, 2012.

APPENDIX A

FMEA SCORING SYSTEM

Table A.1: Table of scoring system for FMEA describing ranking and effect.

Value	**Severity**	**Occurrence**	**Detection**
1	None	Remote	Almost certain
2	Very minor	Very low	Very high
3	Minor	Low	High
4	Very low	Unlikely	Moderately high
5	Low	Marginal	Moderate
6	Moderate	Marginal	Low
7	High	High	Very low
8	Very high	Very high	Remote
9	Hazardous - with warning	Very high	Very remote
10	Hazardous - no warning	Extremely high	Absolute uncertainty